Computer Simulation of Cyclic Block Copolymer Microphase Separation

Hu-Jun Qian, Zhong-Yuan Lu,* Li-Jun Chen, Ze-Sheng Li, and Chia-Chung Sun

State Key Laboratory of Theoretical and Computational Chemistry, Institute of Theoretical Chemistry, Jilin University, Changchun 130023, China

Received October 15, 2004; Revised Manuscript Received December 7, 2004

ABSTRACT: The dissipative particle dynamics (DPD) simulation method is applied to study the mesoscopic phase formation of cyclic diblock copolymer c-A_mB_n ($m + n = 20$). The phase diagram is constructed by simulating at different interaction parameters and composition fractions. The resulted phase diagram is similar to that of the linear diblock copolymer; i.e., the ordered structures such as lamellae, perforated lamellae, hexagonal cylinders, and body-centered-cubic spheres can be identified in the parameter space. Melted structures such as micelle-like, liquid rod, and random network phases have also been found in the phase diagram. The observed $(\chi N)_{ODT}$ is in agreement with the theoretical prediction, if a finite chain length mapping is applied. Cyclization of a linear block copolymer can induce remarkable changes in the morphology of the organized meso structure. This is attributed to the reduced chain length of the cyclic block copolymer. The existence of the melted structures between totally disordered and the ordered phases emphasizes complex dynamical pathway during microphase separations.

1. Introduction

As a fertile source of soft materials, block copolymers attract researchers in both academic and application fields since they have novel properties resulted from their self-organized microphase-separation structures.[1] The synthesis[2] of a block copolymer with a unique architecture, such as star, comb, and ring shape, makes it possible to diversify its applications and investigate the effect of the chain architecture on its physical properties.

Cyclic block copolymer has no chain ends but possesses two junctions between the blocks as compared with the linear block copolymer, which has two or more ends and one junction between the blocks. Therefore, it is expected that the properties of the cyclic block polymers may be different from those of the corresponding linear ones. For example, cyclic polymers are easy to process because they have relatively smaller viscosity compared with the linear polymers. Theoretical studies[3−9] predicted sensitive differences between the properties of the linear and the cyclic copolymer in bulk. For example, Marko[9] predicted an order−disorder transition (ODT) in microphase separation at $\chi N = 17.8$ for a 50/50 cyclic diblock copolymer as compared to the classical result for linear diblock for which $\chi N = 10.5$. It was attributed to the fact that the closed topology suppresses concentration fluctuations. Monte Carlo simulation[10] indicated the effect of the cyclic architecture on ODT by comparing the microphase separation of a symmetric cyclic diblock copolymer with an equivalent linear one. There are also some experimental works about the physical property differences between the cyclic and the corresponding linear block copolymers, both in solution[11−16] and in the bulk.[17−21]

To investigate the phase behavior of a block copolymer system, various techniques had been used, such as dynamical Landau theory,[22,23] self-consistent-field theory (SCFT),[24,25] and the Monte Carlo (MC) method. However, it is difficult to model the equilibrium structures of block copolymers by Landau theory and the SCFT[26,27] because the results of experiments[28] and Monte Carlo[26] simulations indicated that the chain statistics are markedly non-Gaussian nearly up to the critical point. Although by MC, one can both study the equilibrium structures and the dynamical processes;[29−31] unfortunately, there is no hydrodynamic interaction (HI) included, even though HI plays an important role in the kinetics of microphase separation of block copolymers.[32] There is another efficient simulation technique, discontinuous molecular dynamics (DMD), which has been successfully applied to study the phase behavior of linear diblock copolymers.[33] In this method, one need to find the appropriate box length for a specific packing fraction using the box length searching algorithm, but for some specific structures this algorithm is insufficient to find the correct box length. As an alternative choice, in this research, we use the DPD method which is a continuum simulation technique in three dimensions and correctly represents the hydrodynamic interactions.[32] Groot and Madden[34] had successfully applied this method to study the mesophase formation of linear (A_mB_n) diblock copolymer melts. Thus, the DPD simulations of cyclic block copolymers may be needed for directly comparing the results with those of ref 34, also for understanding the speciality of the microdomain formation of the cyclic block copolymers.

In the DPD method, to conserve the momentum, the dissipative forces depend explicitly on the relative velocities of the particles. The velocities, however, also depend on the dissipative forces. This fact makes it difficult to integrate the equations of motion in DPD simulations. To overcome this problem, a number of integration schemes[35−39] have been developed in the past few years. We have tested the four different schemes for computational efficiency. Our results on a system of size $10 \times 10 \times 10$ with particle density $\rho = 3.0$ show that integrating over one time step ($\Delta t = 0.05$) requires 0.03 s for the velocity-Verlet integration scheme (DPD-VV),[36,37] 0.018 s for the modified velocity-Verlet algorithm due to Groot and Warren (GW-VV),[35] 0.028 s for the Shardlow splitting method,[39] and 0.024 s for the Lowe thermostat method[38] ($\Lambda = 5.0$). All these results

* To whom correspondence should be addressed. E-mail: luzhy@mail.jlu.edu.cn.

10.1021/ma0478658 CCC: $30.25
Published on Web 01/27/2005

have been averaged over 30 000 consecutive steps. We can see that the time-consuming of the GW-VV is the lowest, so we use this classical integration scheme in our simulations. The method will be described in the next section.

In this paper, we present the results of DPD simulations of cyclic diblock copolymer systems. The elementary units in DPD method are fluid elements or soft beads. A soft bead represents a volume of fluid that is large on a molecular scale and hence contains at least several molecules or molecular groups, but still macroscopically small.[40] Our block copolymer is modeled by connecting these beads together with the harmonic springs.[35] We have performed the simulations of cyclic chains with $N = 20$ at volume fractions $f = 0.1$, 0.2, 0.3, 0.35, 0.4, and 0.5. Results are summarized in a phase diagram which displays disordered (DIS), quasi-solid body-centered cubic (BCC), hexagonal cylindrical (HEX), and lamellar (LAM) phases in the χN vs f plane. Moreover, we also find melted structures such as micelle-like phase (ML), liquid rod phase (LR), and random network phase (RN). We also find the perforated lamellar (PL) phase which has been found in experiments[41,42] and in DPD simulations[32,34] for linear block copolymers. The observed $(\chi N)_{\mathrm{ODT}}$ is in agreement with the theoretical prediction, if a finite chain length mapping is applied. Cyclization of a linear block copolymer can induce remarkable changes in the morphology of the organized meso structure. This is also attributed to the reduced chain length of the cyclic block copolymer. The existence of the melted structures between totally disordered and the ordered phases emphasizes complex dynamical pathway during microphase separations.

2. Simulation Method and Model Construction

In the DPD method, the time evolution of the interacting particles is governed by Newton's equation of motion.[35] The GW-VV algorithm[34,35] is used here.

$$\begin{aligned}
\mathbf{r}_i(t+\Delta t) &= \mathbf{r}_i(t) + \Delta t\mathbf{v}_i(t) + {}^1\!/_2(\Delta t)^2\mathbf{f}_i(t)\\
\tilde{\mathbf{v}}_i(t+\Delta t) &= \mathbf{v}_i(t) + \lambda\Delta t\mathbf{f}_i(t)\\
\mathbf{f}_i(t+\Delta t) &= \mathbf{f}_i(\mathbf{r}(t+\Delta t), \tilde{\mathbf{v}}(t+\Delta t))\\
\mathbf{v}_i(t+\Delta t) &= \mathbf{v}_i(t) + {}^1\!/_2\Delta t(\mathbf{f}_i(t) + \mathbf{f}_i(t+\Delta t)) \qquad (1)
\end{aligned}$$

We choose $\lambda = 0.65$ and $\Delta t = 0.06$ here according to ref 34.

Interparticle interactions are characterized by pairwise conservative, dissipative, and random forces acting on a particle i by a particle j. They are given by

$$\mathbf{F}_{ij}^C = -\alpha_{ij}\omega^C(r_{ij})\mathbf{e}_{ij} \qquad (2)$$

$$\mathbf{F}_{ij}^D = -\gamma\omega^D(r_{ij})(\mathbf{v}_{ij}\cdot\mathbf{e}_{ij})\mathbf{e}_{ij} \qquad (3)$$

$$\mathbf{F}_{ij}^R = \sigma\omega^R(r_{ij})\xi_{ij}\Delta t^{-1/2}\mathbf{e}_{ij} \qquad (4)$$

where $\mathbf{r}_{ij} = \mathbf{r}_i - \mathbf{r}_j$, $r_{ij} = |\mathbf{r}_{ij}|$, $\mathbf{e}_{ij} = \mathbf{r}_{ij}/r_{ij}$, and $\mathbf{v}_{ij} = \mathbf{v}_i - \mathbf{v}_j$. The ξ_{ij} is a random variable with zero mean and unit variance.

The pairwise conservative force is written in terms of a weight function $\omega^C(r_{ij})$; here we choose $\omega^C(r_{ij}) = 1 - r_{ij}$ for $r_{ij} < 1$ and $\omega^C(r_{ij}) = 0$ for $r_{ij} \geq 1$ such that the forces are soft and repulsive. Unlike the conservative force, the weight functions $\omega^D(r_{ij})$ and $\omega^R(r_{ij})$ of the dissipative and random forces couple together to form a thermostat. Español and Warren[43] showed the relations between the two functions

$$\begin{aligned}
\omega^D(r) &= [\omega^R(r)]^2\\
\sigma^2 &= 2\gamma k_{\mathrm{B}}T \qquad (5)
\end{aligned}$$

This precise relationship between the two forces is determined by the fluctuation−dissipation theorem. We take a simple choice of $\omega^D(r)$ due to Groot and Warren:[35]

$$\omega^D(r) = [\omega^R(r)]^2 = \begin{cases}(1-r)^2 & (r < 1)\\ 0 & (r \geq 1)\end{cases} \qquad (6)$$

It should be noted that the choice of $\omega^D(r_{ij})$ is not unique; the simplest form adopted here is just because of its common usage in roughly all published works.

In our simulations we have chosen the radius of interaction, the particle mass, and the temperature as $r_c = m = kT = 1$ and $\sigma = 3.67$.[34] The particle density ρ is kept equal to 3. According to ref 35, only for sufficiently large density above $\rho > 2$, all simulation systems fall on the same scaling curve of the equation of state. Taking into account the computational efficiency, a low value that $\rho = 3$ is a reasonable choice where the scaling relation still holds. The only parameter to be determined is the conservative interaction strength α_{ij}, which is chosen according to the linear relation with Flory−Huggins χ-parameters:[35]

$$\alpha_{ij} \approx \alpha_{ii} + 3.27\chi_{ij} \qquad (\rho = 3) \qquad (7)$$

Here the interaction parameter between the same bead type α_{ii} equals 25. This value is originated from Groot et al.[34,44] to correctly describe the compressibility of water. Because equal liquid volumes for all components were actually assumed in DPD, the dimensionless compressibility is taken the same value for all components as matched to water at room temperature, and then $\rho\alpha_{ii}/k_{\mathrm{B}}T \approx 75$ is found. The correspondence between the repulsion parameter α and the Flory−Huggins χ parameters places our results in the proper context. It should be noted that by following Groot and Rabone[44] one can quantitatively determine the DPD interaction parameters from the experimental χ parameters or solubility data. Recently, Maiti and McGrother also presented a procedure to coarse-grain a complex fluid from its underlying chemistry.[45] However, in this paper we do not try to relate our results to any particular cyclic block copolymer systems. Instead, we focus on the qualitative phase diagram and the physical speciality due to the particular ring architecture.

Polymers are constructed by connecting the neighboring beads together via the harmonic springs $\mathbf{F}_i^S = \sum_j C\mathbf{r}_{ij}$.[35] We choose the spring constant $C = 4$ according to ref 34. In our simulations, a 3D box of size $20 \times 20 \times 20$ with periodic boundary conditions is adopted. c-A_mB_n is used to represent the cyclic block copolymer, where $m + n = 20$ and the composition fraction of block A is $f = m/(m + n)$.

In a typical simulation, the finite system size may lead to some artificial phases; thus, fine-tuning the box size is crucially important for truly describing the physical properties. In the previous DPD simulations,[32] Groot et al. pointed out that their simulated systems

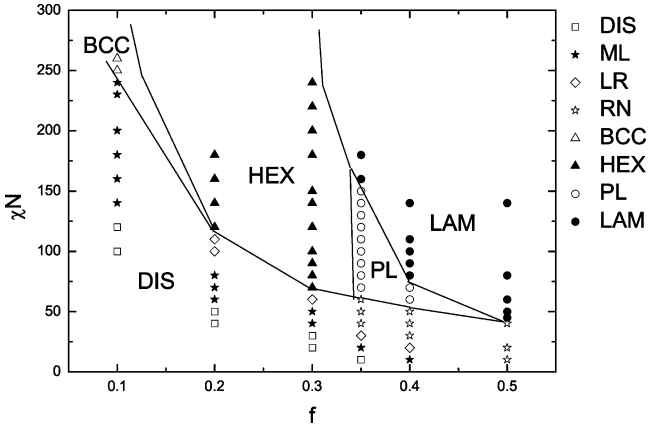

Figure 1. Simulated phase diagram for cyclic block copolymers plotted in χN vs f. Regions of totally disordered phase (DIS), lamellae (LAM), perforated lamallae (PL), hexagonal cylinders (HEX), and body-centered-cubic spheres (BCC) are shown. Between the ordered and the totally disordered regions, we also find some melted structures, such as micelle-like phase (ML), liquid rod phase (LR), and random network (RN). The microphase boundary lines are drawn to guide the eye.

were larger than any of the previous MC simulations. They also adopted a box with size $20 \times 20 \times 20$; however, the chain length $N = 10$. We find that for our cyclic block copolymers ($N = 20$) the mean-squared radius of gyration (R_g^2) almost has the same value as that of the linear ones with the chain length $N = 10$. In addition, the side length of our simulation box is about 10 times larger than the R_g^2 of the cyclic block copolymer with $N = 20$. Therefore, the finite box size effect may not influence our results.

3. Simulation Results and Discussion

We expand our simulation parameter space to include symmetric and asymmetric cyclic block copolymers at different composition fractions and interactions. Therefore, the phase diagram can be constructed, showing disordered, lamellar, perforated lamellar, hexagonal cylindrical, and body-centered-cubic spherical structures. Figure 1 displays the resulting phase diagram, plotted in χN vs f. Note that between the totally disordered region and the ordered phases there are some melted structures, such as micelle-like, liquid rod, and random network. There is no symmetry in these phases; thus, we describe them as droplets (no matter large or small) of the minor moiety in disordered phases. The diagram shows that a direct phase transition occurs between the disordered phase and the lamellar phase at $f = 0.5$. The corresponding $(\chi N)_{ODT}$ is around 45. For moderately asymmetric cyclic block copolymers ($f = 0.4$, 0.35), a perforated lamellar phase is stable below the lamellar phase. For more asymmetric block copolymers ($f = 0.3$, 0.2), cylinders are stable. For highly asymmetric cyclic block copolymers ($f = 0.1$), BCC spheres form above the disordered phase. The typical ordered structures are shown in Figure 2 by calculating the A/B dividing isosurface of equal A and B density. The disordered and melted structures are not shown here.

It is of interest to compare our results with the theoretical predictions and other simulations. Marko[9] had discussed the microphase separation of ring block copolymers using the theory of Leibler[46] with random phase approximation (RPA). He showed that the ordering of ring diblock copolymers was similar to that of linear chains with a reduced chain length. He had also found that for a melt of symmetric diblock rings microphase separation would take place with a demixing interaction larger than $(\chi N)_{ODT} = 17.8$. Following Marko's work, Morozov and Fraaije[47] derived similar expressions for three- and four-monomer probabilities and calculated the nonlinear response properties of ring diblock copolymer melt and obtained its phase diagram. Their resulted phase behavior of the ring diblock copolymer melt is almost the same as that of the linear diblocks with the ODT transition temperature shifted upward. The only difference is a big compositional range $f = 0.33-0.67$ where the direct transition DIS → HEX occurs. This value of $(\chi N)_{ODT}$ can also be located in our simulated phase diagram at the order−disorder transition point of the symmetric cyclic block copolymers. We can see from Figure 1 that, when $\chi N = 40$, the block copolymers are in disordered phase and, when $\chi N = 45$, ordered lamellae appear. Therefore, the value of $(\chi N)_{ODT}$ is in the range of $40 < (\chi N)_{ODT} \leq 45$ in our simulations. Monte Carlo simulation[10] had also been applied to calculate the value of $(\chi N)_{ODT}$. The authors predicted that the value should be in the range of $40.83 < (\chi N)_{ODT} \leq 43.02$. They had also adopted $N = 20$; hence, their result of $(\chi N)_{ODT}$ is in consistent with ours. The discrepancy between our simulated $(\chi N)_{ODT}$ and the Marko's theoretical result may be due to the finite chain length in our simulations and the RPA they used.[8,9]

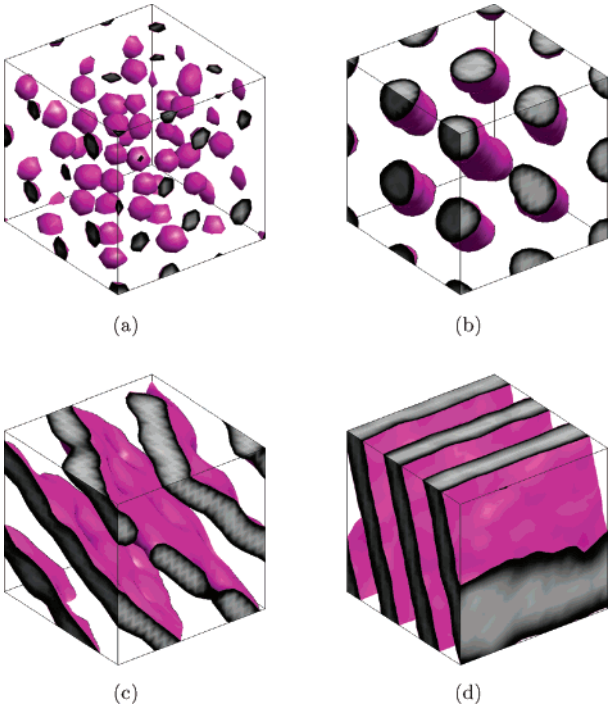

Figure 2. Typical simulated meso-structures for cyclic block copolymers with $N = 20$: (a) BCC at $f = 0.1$ and $\chi N = 260$; (b) HEX at $f = 0.3$ and $\chi N = 180$; (c) PL at $f = 0.35$ and $\chi N = 110$; (d) LAM at $f = 0.5$ and $\chi N = 60$.

Our phase diagram for 20-bead cyclic block copolymers can be compared to Groot and Madden's simulation of 10-bead linear diblock copolymers.[34] They found lamellar, perforated lamellar, hexagonal cylindrical, and BCC spherical phases in the χN vs f plot. Furthermore, they emphesized that the simulation value of $(\chi N)_{ODT}$ was higher than the theoretical prediction. It was attributed to the increasing fluctuation with finite chain length. On the basis of the argument of Fredrickson and Helfand,[48] they gave an expression for calculating an effective χ parameter, $(\chi N)_{eff} = \chi N/(1 + 3.9N^{2/3-2\nu})$,

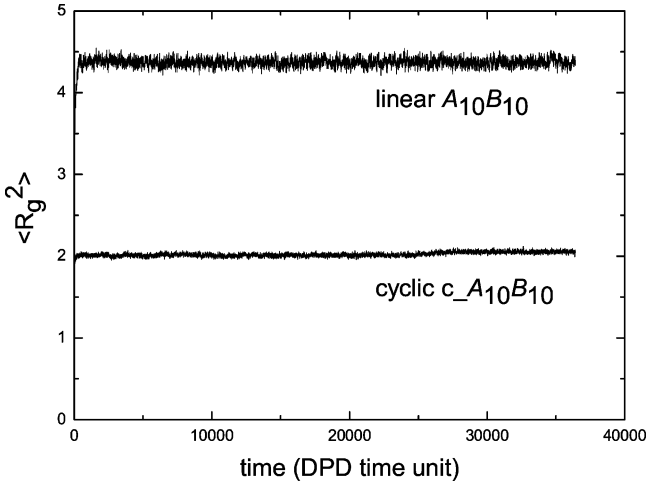

Figure 3. Time evolution of the mean-square radius of gyration for both the cyclic c-A_3B_7 and the linear A_3B_7 block copolymers.

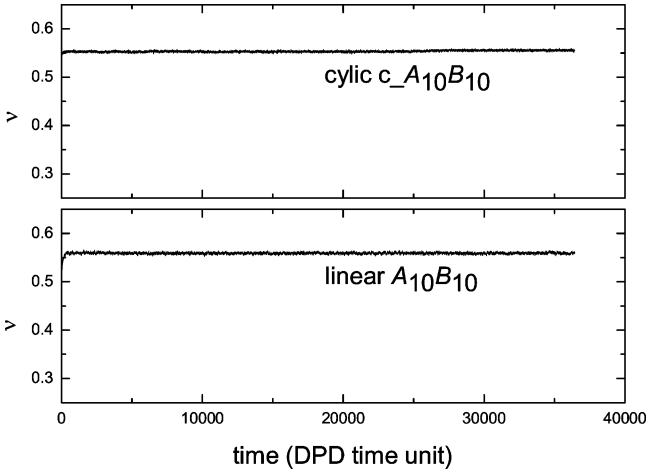

Figure 4. Time evolution of the Flory exponent v, for the cyclic c-$A_{10}B_{10}$ and the linear $A_{10}B_{10}$ block copolymers. In both cases, $\chi N = 45$.

where ν is the Flory exponent. This relation can be used to extrapolate from the finite chain χN to that of the infinitely long chain. However, because this weak coupling relation is not appropriate to cyclic systems, our χN cannot be directly fitted to $(\chi N)_{\text{eff}}$ via the above relation.

Comparing the R_g of the cyclic block copolymer and that of the linear block copolymer, we may do a chain length mapping and give a rough estimate of the $(\chi N)_{\text{ODT}}$ corresponding to the finite chain length of the cyclic block copolymers. The mean-square radius of gyration is defined as

$$\langle R_g^2 \rangle = \left\langle \frac{1}{N} \sum_{i=1}^{N} (r_i - r_{cm})^2 \right\rangle \tag{8}$$

where r_i and r_{cm} denote the position vector of each segment in a chain and the center-of-mass for the whole chain. Figure 3 shows the calculated $\langle R_g^2 \rangle$ for both the cyclic and the linear symmetric block copolymers with $N = 20$ and $\chi N = 45$. It can be easily seen that the chain sizes increase rapidly to the equilibrium from their initial values in both cases. Furthermore, the $\langle R_g^2 \rangle$ of the cyclic block copolymers after equilibrium is nearly half of the corresponding linear ones: $\langle R_g^2 \rangle_{\text{cyclic}} = 0.463 \langle R_g^2 \rangle_{\text{linear}}$. For infinite chain length, we have[49,50]

$$\langle R_g^2 \rangle_{\text{linear}} = \frac{1}{6} N^{2\nu} \langle l^2 \rangle \tag{9}$$

$$\langle R_g^2 \rangle_{\text{cyclic}} = \frac{1}{12} N^{2\nu} \langle l^2 \rangle \tag{10}$$

where $\langle l^2 \rangle$ is the mean-square bond length. These two equations indicate that $\langle R_g^2 \rangle$ of the cyclic chain should be exactly half that of the linear one at infinite chain length. Our simulated result is 0.463, which is only slightly smaller than 0.5, although only $N = 20$ is used here. On the basis of the above relation, we may do a chain length mapping of the cyclic polymer with $N' = 0.463N$ for our systems. Another value for estimating the effective χN is the Flory exponent ν. From eqs 9 and 10, the value of ν is equal to 0.5 if the chains in bulk are Gaussian. Figure 4 shows that ν approaches equilibrium values 0.559 and 0.554 for the linear and cyclic diblock copolymer, respectively. These values are larger than the ideal Gaussian value of 0.5, indicating that the chain conformations in these two cases deviate from the Gaussian state due to the chain expansion at interfaces. From the estimated reduced chain length N' and the Flory exponent ν, we can calculate $(\chi N)_{\text{ODT}}$ for the cyclic block copolymer at finite chain length $N = 20$ via $(\chi N)_{\text{eff}} = \chi N/(1 + 3.9N'^{2/3-2\nu})$, where $(\chi N)_{\text{eff}} = 17.8$.[9] The resulted $(\chi N)_{\text{ODT}} = 43.8$, which is in good agreement with our simulated value and the MC prediction.[10]

According to ref 20, at the same composition fraction and the same polymerization, cyclization of a linear block copolymer induces remarkable changes in the morphology of the organized meso structure. For example, at $f = 0.22$, linear diblock copolymers form a hexagonal phase, whereas the corresponding morphology adopted by cyclic diblock copolymers is a liquidlike micellar phase. Groot and Madden[34] had showed via DPD simulations that, in a box of size $20 \times 20 \times 20$ at density $\rho = 3$ and $\chi N = 46$, the linear block copolymer A_3B_7 evolves into a hexagonal phase after 32 000 DPD time units. Thus, following Groot and Madden, we do the simulations for both linear A_3B_7 and cyclic c-A_3B_7 to compare the difference of their respective meso structures. The results are shown in Figure 5 by calculating the dividing isosurfaces. Linear A_3B_7 forms hexagonal cylinders as shown in Figure 5a, which is in consistent with the result of Groot and Madden. The result for the c-A_3B_7 is a structure with randomly distributed micelles as shown in Figure 5b, which is in agreement with the experiment observation.[20] The different meso structure of c-A_3B_7 emphasizes the speciality of the cyclic block copolymer due to its particular ring architecture. This difference may also be understood with a chain length mapping as we have described above. Suppose that $(\chi N)_T$ is the threshold for HEX appearance of the linear block copolymers. c-A_3B_7 with $N = 10$ corresponds to a linear block copolymer with roughly chain length $N' = 5$; thus, $(\chi N)_T$ shifts to larger value in this case according to $(\chi N)_{\text{eff}} = \chi N/(1 + 3.9N'^{2/3-2\nu})$. Subsequently, we may observe micellar structure (cf. Figure 1) for c-A_3B_7 at the same χN with which linear A_3B_7 resides in the HEX phase. As an addition, we have done some extra simulations for cyclic copolymers with chain length $N = 10$ at volume fraction $f = 0.4$, 0.35, and 0.14 and compared these results with those of linear ones given by Groot and Madden.[34] All these comparisons are listed in Table 1. Our results

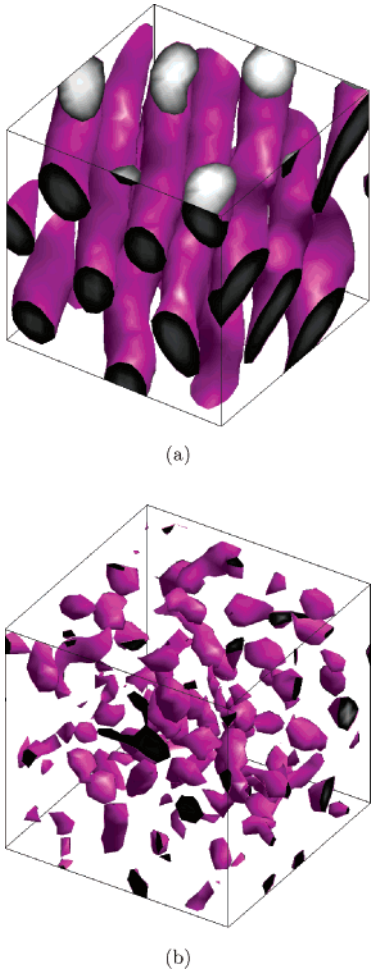

Figure 5. Morphology of linear A_3B_7 and cyclic c-A_3B_7 diblock copolymer systems obtained after 5.4×10^5 steps simulation with $\chi N = 46$ and $\rho = 3$. (a) Hexagonal phase for the linear system. (b) Dividing isosurface of cyclic block copolymer c-A_3B_7, which shows a micelle-like phase.

Table 1. Input Parameters and Resulted Meso-Phases for All Comparison Runs between Cyclic and Corresponding Linear Block Copolymers[a]

description	f	α_{ij}	χN	time	phase
A_1B_9/A_2B_8	0.14	57	98	64 000	bcc
A_3B_7	0.30	40	46	30 000	hexagonal
A_3B_7/A_4B_6	0.35	40	46	32 000	perforated lamellar
A_4B_6	0.40	40	46	30 000	lamellar
c-A_1B_9/c-A_2B_8	0.14	57	98	64 000	micelle-like
c-A_3B_7	0.30	40	46	32 400	micelle-like
c-A_3B_7/c-A_4B_6	0.35	40	46	36 000	random networks
c-A_4B_6	0.40	40	46	36 000	random networks

[a] The particle density $\rho = 3$ and box size is $20 \times 20 \times 20$. The fraction of A beads in the system is denoted by f. The repulsion parameter between the equal beads is $\alpha_{ii} = 25$, and for the unequal beads this parameter is denoted by α_{ij}. Time refers to the simulation time in the units of $r_c\sqrt{m/k_BT}$, where r_c is the interaction radius. All the results for linear block copolymers are from ref 34.

provide further motivations for experimentally probing the different morphologies of cyclic block copolymers which has not been performed so far.

We have also investigated the morphology differences between cyclic and linear block copolymers and compared the domain sizes during the microphase separation. The mean-square distances between the centers-of-mass of blocks A and B, $\langle D^2 \rangle$, are calculated for both the cyclic c-$A_{10}B_{10}$ and the linear $A_{10}B_{10}$ systems. This

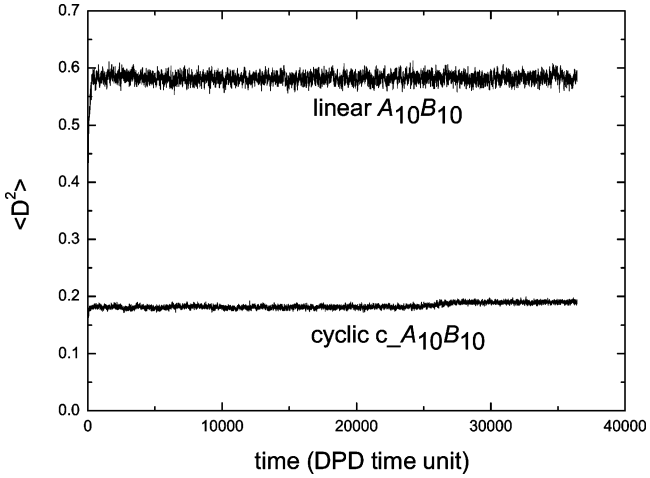

Figure 6. Time evolution of the mean-square distance between the centers-of-mass of blocks A and B, $\langle D^2 \rangle$, for both the cyclic c-$A_{10}B_{10}$ and the linear $A_{10}B_{10}$ block copolymers.

mean-square distance is defined as $\langle D^2 \rangle = \langle (r_{A,cm} - r_{B,cm})^2 \rangle$. Figure 6 shows the time evolution of $\langle D^2 \rangle$ for both systems. We can see that this value converges to 0.184 for the cyclic block copolymer and is much smaller than 0.582 for the linear one. This is also due to the ring-shape architecture, which increases the number of contacts between the repulsive segments A and B and thus decreases the dimension size of the chains microscopically and the domain size at the mesoscopic scale. The ratio of the periodic domain spacing between the cyclic diblock copolymer and the linear chain is estimated to be 0.67. This value is comparable to the value predicted by the MC simulation.[10] The half chain segment−segment distances (HCSSD) for both c-$A_{10}B_{10}$ and $A_{10}B_{10}$ are also calculated at $\chi N = 45$ and 400, respectively. We then do a Gaussian fit of HCSSD and compare the chain size differences at the weak and strong segregation conditions. At $\chi N = 45$, the most probable value of HCSSD is 3.57 ± 0.02 for $A_{10}B_{10}$ and 2.54 ± 0.01 for c-$A_{10}B_{10}$, while at $\chi N = 400$, we have 4.14 ± 0.02 and 2.98 ± 0.01, respectively. These approximate values show that both kinds of chains are more stretched at the strong segregation condition, although in this case Gaussian fitting may not be valid anymore.

We observe the perforated lamellar (PL) phase between the cylindrical and lamellar phases at $f = 0.35$ and 0.4, whereas the SCFT theory predicts a stable gyroid phase in this region.[51] Contrary to the theoretical predictions, some experimental studies of copolymers[52−54] are more consistent with our simulation results. They found that the PL phase is stable[52,53] or metastable.[54] However, the existence of PL phase may be possible because of our finite simulation box size.[33] To test this, we do a simulation with the box size $25 \times 25 \times 25$ at $f = 0.35$ and $\chi N = 140$ for long times. This system should be large enough for the gyroid phase to form without the finite box size effect, but still no gyroid structure is found. Another interesting thing should also be mentioned here is that the perforations in our PL structures are not always hexagonally spaced, which is in agreement with the DMD results for linear block copolymers.[33] At $f = 0.4$, perforations are small and transient and without any symmetry. At volume fractions $f = 0.35$, the perforations are larger, more stable, and hexagonally ordered. The absence of gyroid phase in a

DPD simulation may inherently relate to the method itself.

When the volume fraction f is at 0.2 and 0.3, we obtain the hexagonal cylinders. According to ref 32, hexagonal cylinders form via a metastable gyroid-like structure and therefore correspond to the nucleation-and-growth mechanism, whereas the lamellar phase is formed via a spinodal decomposition. Consequently, the hexagonal phase appears with an order of magnitude slower than the lamellar phase, so longer simulation times have been used at $f = 0.2$ and 0.3 in this work. At the strong segregation region when $f = 0.3$, such as at $\chi N = 220$ and 240, a connected tube structure may appear instead of the expected hexagonal cylinder phase. But when we start the simulation from the hexagonal configuration obtained in a smaller χN simulation, the HEX cylinders will be perfected and stabilized. Therefore, these two points at $f = 0.3$ with $\chi N = 220$ or 240 are also in the region of hexagonal cylindrical phase. The appearance of the connected tubes indicates that the system get stuck into a local minimum in free energy surface. After the connected tubes are formed, the connections cannot be broken despite long simulation times. This shows that there are high barriers between the local and the global minima, and the system cannot easily jumped over the barrier. It may be due to the strong repulsions between blocks A and B. Such high repulsions make it difficult to rupture the connections between the tubes.

In our phase diagram, there are also some melted structures in the region between the totally disordered and the ordered phases. These structures were found for linear block copolymers by Groot and Madden.[34,32] They distinguished processes on three different length and time scales in the formation of polymer mesophases: (1) phase separation on the mesoscopic bead level, (2) organization of polymers into micelles, and (3) the organization of these micelles into a superstructure with its own particular symmetry (cf. Figure 2 of ref 34). In our phase diagram, at $f = 0.1$, a micelle-like phase is found between the disordered and BCC phases. This corresponds to the level 1 ordering in Groot and Madden's scheme. At $f = 0.2$ and 0.3, the micelle-like phase is also found above the totally disordered phase, and after that, another type of melted structure, liquid rod phase, is found before the ordered hexagonal phase. This may correspond to the level 2 ordering. At $f = 0.35$, 0.4, and 0.5, we find a percolation of the minority phase into a random network, as shown in our simulated phase diagram. Moreover, the level 3 ordering corresponds to the formation of the final ordered superstructures. The appearance of these melted structures further testifies the advantage of DPD that can trace the complex dynamic processes in the formation of polymer microphases.

In typical DPD, the bond crossing is needed. If the chain topology is conserved during the simulation, the phase separation phenomena may differ from our present results. This is because the segmental movement during microphase separation is restricted severely especially in the cyclic diblock copolymers if bond crossing is not allowed. For this reason, it is necessary to test whether bond crossing can happen in our simulations with any χN. Figure 7 shows two typical initially interlinked loop polymers during the simulation. For example, parts a and b of Figure 7 show the chain conformations of cyclic c-$A_{10}B_{10}$ at $\chi N = 60$ after 2×10^4 and 4×10^4 integration steps, respectively. Parts c and d of Figure 7 show the cyclic c-A_2B_{18} at $\chi N = 400$ after 2×10^4 and 4×10^4 integration steps, respectively. After short time simulation, the interlinked loop polymers separate from each other no matter whether χN is small or not. This shows that the bond crossing is always allowed in our simulations. Although it is unphysical, bond crossing together with the soft interaction is the merit of the DPD, which can significantly speed up the equilibrium of the system. Of course, one can disallow the bond crossability,[55] if the realistic dynamic process during the phase separation is emphasized. However, in this case the efficiency of DPD will be sacrificed, which is against the idea of DPD. In the spirit of multiscale simulation, we may need to combine the virtue of both coarse-grained and atomistic methods for obtaining a clear overview of the microphase separation of block copolymers.

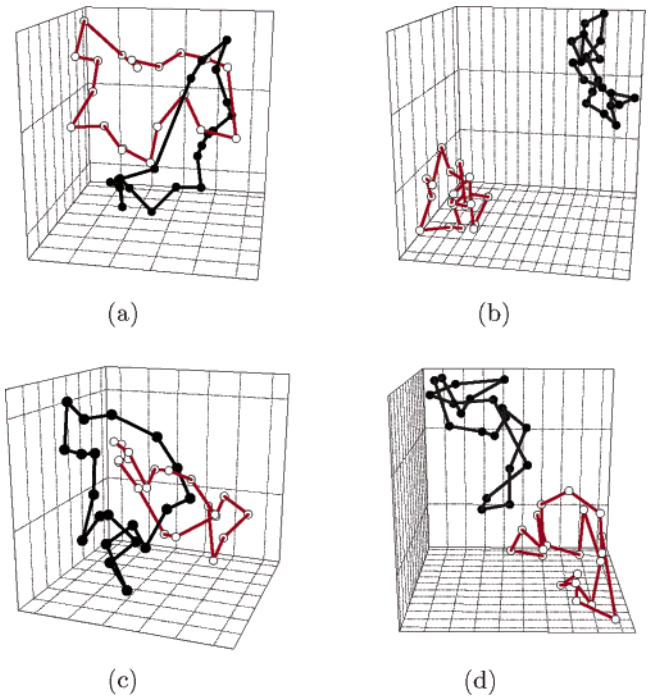

Figure 7. Chain conformations during the simulations of the cyclic block copolymers: (a) c-$A_{10}B_{10}$ at $t = 1200$ and $\chi N = 60$; (b) c-$A_{10}B_{10}$ at $t = 2400$ and $\chi N = 60$; (c) c-A_2B_{18} at $t = 1200$ and $\chi N = 400$; (d) c-A_2B_{18} at $t = 2400$ and $\chi N = 400$.

4. Conclusions

The behavior of the microphase separation of cyclic diblock copolymers is investigated via the dissipative particle dynamics by varying composition fraction and value of χ at the fixed chain length $N = 20$. Our simulated phase diagram shows similar ordered structures as those of the linear ones, such as lamellae, perforated lamellae, hexagonal cylinders, and body-centered-cubic spheres. By locating the order−disorder transition point in our phase diagram, we find the ODT region $40 < (\chi N)_{ODT} \leq 45$, which is consistent with the MC results. The theoretical value of $(\chi N)_{ODT} = 17.8$ corresponds to infinite chain length. Thus, we do a mapping of this value to obtain $(\chi N)_{ODT}$ of the finite length cyclic block copolymer. The resulted $(\chi N)_{ODT} = 43.8$ is in good agreement with our simulated value.

By comparing the microphase morphology of linear A_3B_7 and cyclic c-A_3B_7 diblock copolymers, we find that the cyclization of a linear block copolymer can induce remarkable changes in the organized meso structures,

which is in harmony with the experiment observations. This is attributed to the reduced chain length of the cyclic block copolymer.

In the region between the totally disordered and ordered phases, we find some melted structures, such as micelle-like, liquid rod, and random network phases. These melted structures further demonstrate the complex dynamical pathway during microphase separations.

Acknowledgment. This work is supported by the National Science Foundation of China (20490220, 20404005).

References and Notes

(1) Bucknall, D. G.; Anderson, H. L. *Science* **2003**, *302*, 1904.
(2) Pitsikalis, M.; Pispas, S.; Mays, J. W.; Hadjichristidis, N. *Adv. Polym. Sci.* **1998**, *135*, 1.
(3) Benmouna, M.; Borsali, R.; Benoît, H. *J. Phys. II* **1993**, *3*, 1401.
(4) Borsali, R.; Benmouna, M. *Europhys. Lett.* **1993**, *23*, 263.
(5) Borsali, R.; Benmouna, M.; Benoît, H. *Physica A* **1993**, *201*, 129.
(6) Benmouna, M.; Borsali, R. *J. Polym. Sci., Part B: Polym. Phys.* **1994**, *32*, 981.
(7) Borsali, R.; Benmouna, M. *Makromol. Chem. Symp.* **1994**, *79*, 153.
(8) Borsali, R.; Lecommandoux, S.; Pecora, R.; Benoît, H. *Macromolecules* **2001**, *34*, 4229.
(9) Marko, J. F. *Macromolecules* **1993**, *26*, 1442.
(10) Jo, W. H.; Jang, S. S. *J. Chem. Phys.* **1999**, *111*, 1712.
(11) Merkle, G.; Burchard, W.; Lutz, P.; Freed, K. F.; Gao, J. *Macromolecules* **1993**, *26*, 2736.
(12) Amis, E. J.; Hodgson, D. F.; Wu, W. *J. Polym. Sci., Part B: Polym. Phys.* **1993**, *31*, 2049.
(13) Vlahos, C.; Hadjichristidis, N.; Kosmas, M. K.; Rubio, M.; Freire, J. J. *Macromolecules* **1995**, *28*, 6854.
(14) Yu, G.-E.; Carrett, C.-R.; Mai, S.-M.; Altinok, H.; Attwood, D.; Price, C.; Booth, C. *Langmuir* **1998**, *14*, 2278.
(15) Iatrou, H.; Hadjichristidis, N. *Macromolecules* **2002**, *35*, 5426.
(16) Minatti, E.; Viville, P.; Borsali, R.; Schappacher, M.; Deffieux, A.; Lazzaroni, R. *Macromolecules* **2003**, *36*, 4125.
(17) Lescanec, R. L.; Hajduk, D. A.; Kim, G. Y.; Gan, Y.; Yin, R.; Gruner, S. M.; Hogen-Esch, T. E.; Thomas, E. L. *Macromolecules* **1995**, *28*, 3485.
(18) Zhu, Y. Q.; Gido, S. P.; Iatrou, H.; Hadjichristidis, N.; Mays, J. W. *Macromolecules* **2003**, *36*, 148.
(19) Takano, A.; Kardoi, O.; Hirahara, K.; Kawahara, S.; Isono, Y.; Suzuki, J.; Matsushita, Y. *Macromolecules* **2003**, *36*, 3045.
(20) Lecommandoux, S.; Borsali, R.; Schappacher, M.; Deffieux, A.; Narayanan, T.; Rochas, C. *Macromolecules* **2004**, *37*, 1843.
(21) Matsushita, Y.; Iwata, H.; Asari, T.; Uchida, T.; ten Brinke, G.; Takano, A. *J. Chem. Phys.* **2004**, *121*, 1129.
(22) Qi, S.; Wang, Z. G. *Phys. Rev. E* **1997**, *55*, 1682.
(23) Goveas, J. L.; Miller, S. T. *Macromolecules* **1997**, *30*, 2605.
(24) Laradji, M.; Shi, A. C.; Noolandi, J.; Desai, R. C. *Macromolecules* **1997**, *30*, 3242.
(25) Matsen, M. W. *Phys. Rev. Lett.* **1998**, *80*, 4470.
(26) Fried, H.; Binder, K. *J. Chem. Phys.* **1991**, *94*, 8349.
(27) Larson, R. G. *Macromolecules* **1994**, *27*, 4198.
(28) Almdal, K.; Rosedale, J. H.; Bates, F. S.; Wignall, G. D.; Fredrickson, G. H. *Phys. Rew. Lett.* **1990**, *65*, 1112.
(29) Dotera, T.; Hatano, A. *J. Chem. Phys.* **1996**, *105*, 8413.
(30) Hoffman, A.; Sommer, J.-U.; Blumen, A. *J. Chem. Phys.* **1997**, *107*, 7559.
(31) Pakula, T.; Karatasos, K.; Anastasiadis, S. H.; Fytas, G. *Macromolecules* **1997**, *30*, 8463.
(32) Groot, R. D.; Madden, T. J.; Tildesley, D. J. *J. Chem. Phys.* **1999**, *110*, 9739.
(33) Schultz, A. J.; Hall, C. K.; Genzer, J. *J. Chem. Phys.* **2002**, *117*, 10329.
(34) Groot, R. D.; Madden, T. J. *J. Chem. Phys.* **1998**, *108*, 8713.
(35) Groot, R. D.; Warren, P. B. *J. Chem. Phys.* **1997**, *107*, 4423.
(36) Besold, G.; Vattulainen, I.; Karttunen, M.; Polson, J. M. *Phys. Rev. E* **2000**, *62*, R7611.
(37) Vattulainen, I.; Karttunen, M.; Besold, G.; Polson, J. M. *J. Chem. Phys.* **2002**, *116*, 3967.
(38) Lowe, C. P. *Europhys. Lett.* **1999**, *47*, 145.
(39) Shardlow, T. *SIAM J. Sci. Comput.* **2003**, *24*, 1267.
(40) Shillcock, J. C.; Lipowsky, R. *J. Chem. Phys.* **2002**, *117*, 5048.
(41) Hamley, I. W.; Koppi, K. A.; Rosedale, J. H.; Bates, F. S.; Almdal, K. A.; Mortensen, K. *Macromolecules* **1993**, *26*, 5959.
(42) Zhao, J.; Majumda, B.; Schulz, M. F.; Bates, F. S.; Almdal, K.; Mortensen, K.; Hajduk, D. A.; Gruner, S. M. *Macromolecules* **1996**, *29*, 1204.
(43) Español, P.; Warren, P. B. *Europhys. Lett.* **1995**, *30*, 191.
(44) Groot, R. D.; Rabone, K. L. *Biophys. J.* **2001**, *81*, 725.
(45) Maiti, A.; McGrother, S. *J. Chem. Phys.* **2004**, *120*, 1594.
(46) Leibler, L. *Macromolecules* **1980**, *13*, 1602.
(47) Morozov, A. N.; Fraaije, J. G. E. M. *Macromolecules* **2001**, *34*, 1526.
(48) Fredrickson, G. H.; Helfand, E. *J. Chem. Phys.* **1987**, *87*, 697.
(49) Kramers, H. A. *J. Chem. Phys.* **1946**, *14*, 415.
(50) Zim, B. H.; Stockmayer, W. H. *J. Chem. Phys.* **1949**, *17*, 1301.
(51) Matsen, M. W.; Bates, F. S. *J. Chem. Phys.* **1997**, *106*, 2436.
(52) Almdal, K.; Koppi, K. A.; Bates, F. S.; Mortensen, K. *Macromolecules* **1992**, *25*, 1743.
(53) Khandpur, A. K.; Förster, S.; Bates, F. S.; Hamley, I. W. *Macromolecules* **1995**, *28*, 8796.
(54) Hajduk, D. A.; Takenouchi, H.; Hillmyer, M. A.; Bates, F. S. *Macromolecules* **1997**, *30*, 3788.
(55) Pan, G.; Manke, C. W. *Int. J. Mod. Phys. B* **2003**, *17*, 231.

MA0478658